ELSEVIER

Sensors and Actuators 77 (1999) 167–177

SENSORS AND ACTUATORS A PHYSICAL

www.elsevier.nl/locate/sna

A micromachined pressure/flow-sensor

R.E. Oosterbroek *, T.S.J. Lammerink, J.W. Berenschot, G.J.M. Krijnen, M.C. Elwenspoek, A. van den Berg

Department of Electrical Engineering, MESA Research Institute, University of Twente, PO Box 217, 7500 AE Enschede, Netherlands

Received 13 October 1998; received in revised form 3 March 1999; accepted 8 March 1999

Abstract

The micromechanical equivalent of a differential pressure flow-sensor, well known in macro mechanics, is discussed. Two separate pressure sensors are used for the device, enabling to measure both, pressure as well as volume flow-rate. An integrated sensor with capacitive read-out as well as a hybrid, piezo-resistive variant is made. The fabrication processes are described, using silicon and glass processing techniques. Based on the sensor layout, equations are derived to describe the sensor behavior both statically as well as dynamically. With the derived equations, the working range of the sensor and the thermal and time stability is estimated. The computed results of the stationary behavior are verified with the measured data. A good similarity in linearity of the pressure/flow relation is found. The computed hydraulic resistance, however, differs from the measured value for water with 21%. This difference can be explained by the high sensitivity of the resistance to the resistor channel cross-section parameter in combination with the difference between the rounded etched shape and the rectangular approximation. From fluid dynamics simulations, a working range bandwidth of about 1 kHz is expected. Thermal influences on the sensor signal due to viscosity changes are in the order of 2% flow signal variation per Kelvin. From these results, it can be concluded that the sensor can be used as a low cost, low power consuming flow and pressure-sensing device, for clean fluids without particles and without the tendency to coat the channel walls. If a high accuracy is wanted, an accurate temperature sensing or controlling system is needed. © 1999 Elsevier Science S.A. All rights reserved.

Keywords: Flow-sensors; Pressure-sensors; Modeling

1. Introduction

In the area of integrated fluid analysis systems such as μ-TAS (micro total analysis system), liquid or gas flows need to be measured and controlled [1–3]. The flows can be dosed by using, for instance, regulated micro pumps and active valves [4–6]. To adapt the flow delivery to changing impedances and to know exactly the parameters, at which it is delivered, sensors are needed. The parameter of interest for feeding the chemical detection system is mass flow. Pressure is the complementary parameter, needed to compute the applied hydraulic power. In this paper is discussed the pressure/flow-sensor, which can sense both parameters and therefore deliver all relevant information for flow and pressure delivery in a μ-TAS. The pressure is measured with capacitive or piezo-resistive pressure sensors, whereas the flow rate is computed from the pressure drop over a well defined, hydraulic resistance. Design formulas, the static and dynamic behavior and the resulting advantages and drawbacks are discussed.

2. The flow sensing principle

The flow sensing principle of the pressure/flow-sensor is to measure the pressure drop over a hydraulic resistor. Deriving the flow-rate out of this differential pressure signal is well known. There are two ways to obtain a relation. A conversion of kinetic energy (speed) to potential energy (pressure) can be accomplished by leading the flow through a converging/diverging nozzle such that the speed is increased locally. Measuring the dynamic and static pressure and using the relation between pressure and velocity according to Bernoulli gives the fluid speed [7]. This principle is used in venturi type macro flow-sensors and is only applicable when no substantial energy losses due to friction are expected. For micro channels with liquid flows at low Reynolds values, this energy loss cannot be neglected. Therefore, we chose for measuring

* Corresponding author. Tel.: +31-53-489-2-718; Fax: +31-53-4893-343; E-mail: r.e.oosterbroek@el.utwente.nl

0924-4247/99/$ - see front matter © 1999 Elsevier Science S.A. All rights reserved.
PII: S0924-4247(99)00188-0

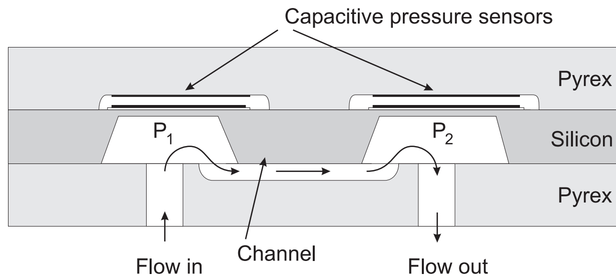

Fig. 1. Schematic view of the lay-out of the integrated capacitive pressure/flow-sensor, fabricated with bulk micromachining techniques.

the pressure loss over a hydraulic resistance [8]. This means that the sensor is passive and a small amount of hydraulic energy is extracted from the fluid flow and transformed into a pressure drop signal. The principle is similar to the well-known use of an electrical shunt resistor to convert current into a measurable voltage drop.

3. Fabrication

The functional layout of the sensor is drawn in Fig. 1. To guarantee that the static pressure instead of the dynamic pressure is measured, the fluid velocity in the resistor must be much higher than at the points where pressure is measured. Therefore, two chambers, one at the entrance and one at the exit, are needed. The space required for the pressure sensor membranes can be used for this.

For the micro pressure/flow-sensor, we made two prototypes, one hybrid design, consisting of two piezo-resistive sensor dies, glued on top of a $10 \times 5 \times 0.9$ mm glass–silicon substrate, embedding the resistor channel and a fully, $10 \times 5 \times 1.4$ mm integrated design with capacitive pressure sensors. Fig. 2 shows a schematic view of the hybrid variant. With an-isotropic KOH etching, holes were made through ⟨100⟩ oriented silicon. After the resistor channels are isotropically etched in the glass wafer with HF, using chromium as a mask layer, holes are created through the wafer, using a powder blasting process. With the use of the anodic bonding process, the glass wafer is

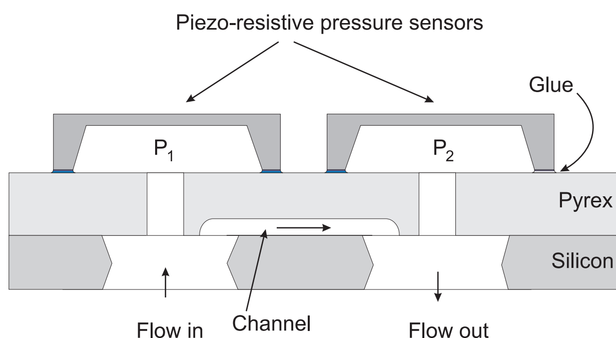

Fig. 2. Lay-out of the hybrid variant of the pressure/flow-sensor, using piezo-resistive pressure-sensors.

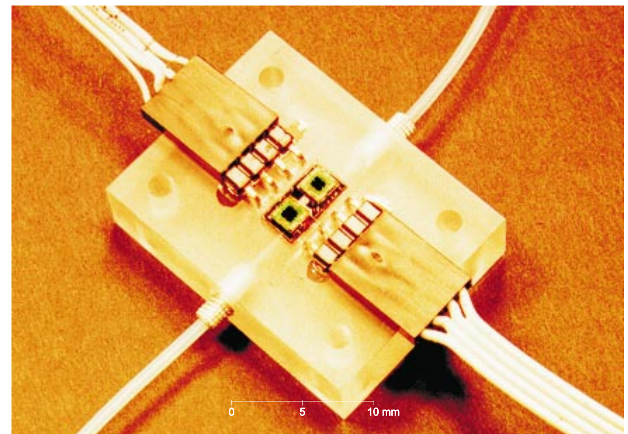

Fig. 3. Mounted hybrid pressure/flow-sensor with electrical connectors and tubing.

mounted on the silicon wafer. A stamping method is used to pattern glue accurately on the pressure-sensor dies (~ 100 μm precision), after which the dies are mounted on top of the glass–silicon sandwich. Finally, the dies are mounted on a 'system board' and electrical and fluidic connections are made (Fig. 3).

Since the sensor principle is passive and needs no actuation power, a low power version is designed by replacing the piezo-resistive pressure sensors by capacitive transducers. For this, a fully integrated design has been made. Figs. 1 and 4 show the cross-sections. The sensor is built in a glass–silicon–glass sandwich structure. In the bottom glass wafer, the hydraulic resistors are etched, again using isotropic HF etching in combination with a chromium mask (Fig. 5, sequence C). After this, holes through the glass are created.

The top wafer holds the upper, fixed electrodes for reading-out the membrane deformations as a function of the applied pressure. By depositing the electrodes in a cavity, the initial gap between the electrodes is defined. The process steps used for this are drawn in Fig. 5,

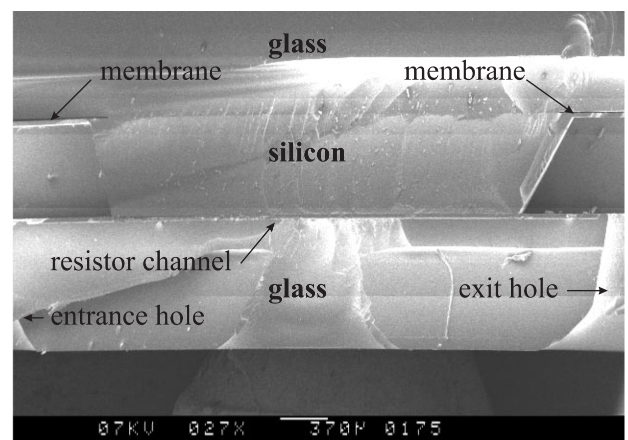

Fig. 4. SEM picture of the cross-section of the integrated capacitive pressure/flow-sensor.

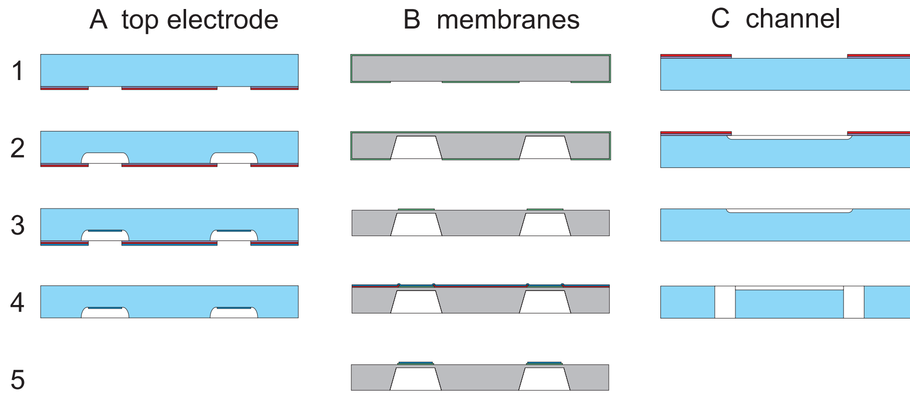

Fig. 5. Process sequence of the integrated capacitive pressure/flow-sensor: (A) top electrode with combined etch/shadow mask, (B) membrane + lower electrode fabrication, and (C) hydraulic resistor processing.

sequence A. The first step (A1) consists of patterning a chromium mask layer by means of a wet chromium etching technique. After the glass is etched in HF such that the cavities have reached the required depth (A2), chromium and platinum are deposited (A3). Since the resist–chromium mask is under etched during the HF step, the mask is used as a shadow mask as well, such that the edges of the top electrode are well defined inside of the cavity. With this combined etch and shadow mask, the electrode material is only deposited at the bottom such that short-circuiting of the electrical connections is avoided. After stripping the resist/chromium layers in HNO_3, the glass wafer with the top electrodes is finished.

The silicon wafer contains the membranes and complementary electrodes for the pressure sensors. First, the membranes are etched anisotropically in a KOH solution, using silicon nitride as mask and defining the membrane thickness by a stop in time (steps B1–2). After this, the silicon nitride at the membrane side is removed at areas that need to be bonded and the lower electrodes are patterned with a lift-off technique.

For bonding the two glass wafers with the silicon wafer, the anodic bonding method is used. Because the distance between the upper and lower electrodes is rather small, the electrostatic forces on the membranes during the bonding process could damage the sensor. Therefore, all upper and lower electrodes are connected to the same potential, resulting in a potential drop between the glass and silicon only. Dicing of the sensors is done such that the connections to the upper and lower electrodes become accessible. For this, a V-groove is etched in the silicon and the top and bottom glass wafers are partly diced at a shifted

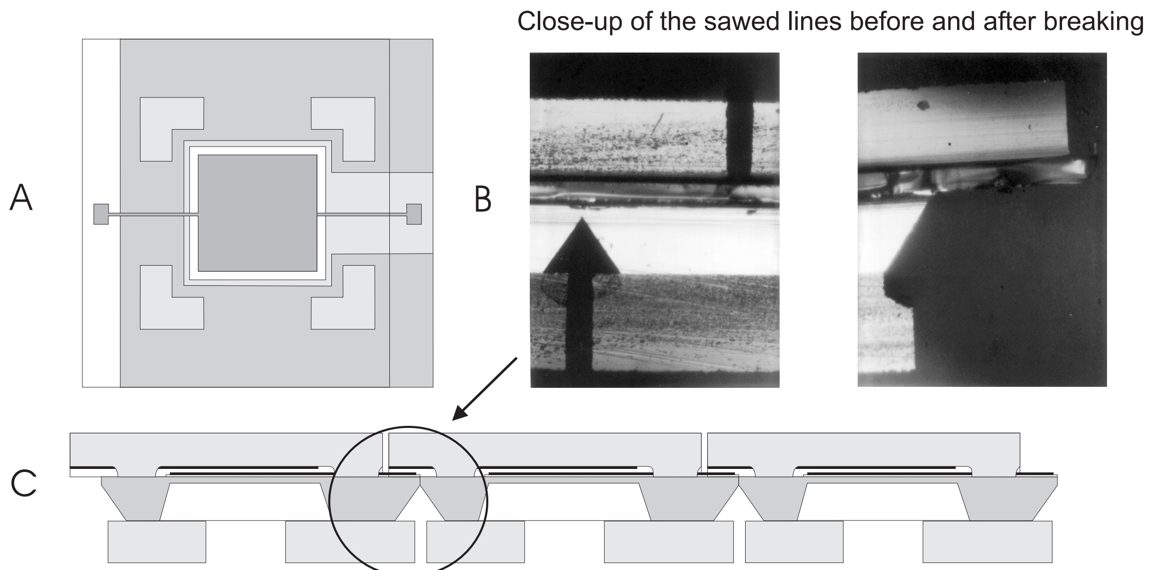

Fig. 6. Dicing method to free the entrance to the electrodes: (A) Top-view of half of the sensor (one pressure sensor only), (C) Combination of saw-lines and v-grooves. After breaking, the upper electrode becomes accessible as shown in the photos (B).

Table 1
Dimensional parameters and units used for the membrane theory and capacitance calculation

Membrane theory	Parameter or constant	Units	Capacitance	Parameter or constant	Units
Pressure	p	N/m^2	Capacitance	c	c^2/Nm
Deflection	w	m	Dielectric constant of vacuum	ε_0	c^2/Nm^2
Center deflection	w_0	m	Relative dielectric constant	ε_r	–
Thickness	h	m	Area	s	m^2
Radius	a	m	Gap distance	d	m
Length	$2a$	m	Gap distance (unloaded)	d_0	m
Radius coordinate.	r	m	Inner electrode radius	r_{c1}	m
Angular coordinate	θ	rad	Outer electrode radius	r_{c2}	m
x–y coordinates	x, y	m	Outer x-coordinate electrode	x_c	m
Modulus of elasticity	E	N/m^2	Outer y-coordinate electrode	y_c	m
Poisson's constant	ν	–	Electrode area	S_c	m^2
Pre-stress	σ_0	N/m^2			

position. After breaking, the bond pads become accessible, as shown in Fig. 6.

4. Modeling of the stationary sensor behavior

4.1. Pressure-sensor membranes

Varying the resistors and/or the dimensions of the sensor membranes makes it possible to adapt the sensor for a specific flow and pressure range. To predict the effects of the different design parameters, we derived simple design formulas for the fluid mechanical and structural mechanical behavior. Only the fully integrated capacitive pressure/flow-sensor will be discussed, since commercially available pressure sensor dies were used for the piezo-resistive variant.

The used parameters are summarized in Table 1. The capacitance/pressure relation of the sensors is defined by, among others, the stiffness of the membranes. For small deflections the dimensionless linear pressure/deflection membrane formula (1) can be used [9,10]:

$$Q = K_b W_0 \tag{1}$$

The parameter definitions are given in Table 2. Q is a dimensionless load parameter, K_b the bending stiffness and W_0 the center deflection of the membrane relative to the membrane thickness. Relation (1) fits well for deflections W_0, smaller than about 0.5. For values of W_0 larger than 0.5, the in-plane stresses become important resulting in a non-linear load deflection relation. A simple approximation for these situations with additional pre-stress is given by:

$$Q = K_\sigma W_0 + K_d W_0^3. \tag{2}$$

In this relation, K_σ is the pre-stress term whereas K_d represents the net stiffness constant when in-plane stresses become important. For circular and square membranes, the definitions of the stiffness constants differ. Analytical and numerical results have been presented in literature [9,10].

To compute the electric and hydraulic capacitance of the pressure sensor, the deflection shape of the membrane is needed. For round membranes, the spherical relation is given by:

$$W = W_0 (1 - R^2)^2. \tag{3}$$

For square membranes, the deflection as well as the clamped edges are described by the spherical relation:

$$W = W_0 (1 - X^2)^2 (1 - Y^2)^2 \tag{4}$$

4.2. Electric pressure-sensor capacitance

The electric capacitance of the pressure sensor varies when pressure is applied on the membranes due to the changing gap geometry between the upper and lower

Table 2
Definition of the introduced dimensionless membrane and capacitance parameters

Membrane theory	Parameter	Elements	Capacitance	Parameter	Elements
Load	Q	pa^4/Eh^4	Specific capacitance	C	$ch/\varepsilon a^2$
Deflection	W	w/h	Gap distance (unloaded)	D_0	d_0/h
Center deflection	W_0	w_0/h	Inner electrode radius	R_{c1}	r_{c1}/a
Radius coordinate	R	r/a	Outer electrode radius	R_{c2}	$r_c 2/a$
Angular coordinates	θ	θ	Outer electrode x coordinate	X_c	x_c/a
x–y coordinates	X,Y	$x/a,\ y/a$	Outer electrode y coordinate	Y_c	y_c/a

electrode. This pressure/capacitance relation can be approximated by the surface integral given in Eq. (5).

$$c=\int_{S_c}\frac{\varepsilon_0\varepsilon_r}{d}\mathrm{d}s=\varepsilon_0\varepsilon_r\int_{S_c}\frac{1}{d}\mathrm{d}s \tag{5}$$

With d the gap distance between the upper and lower electrodes as a function of the position and the electrode area. Substitution of the shape function of a round membrane results in the dimensionless deflection/capacity relation (6), where the circular electrode ranges from $R=R_{c1}$ to R_{c2}.

$$c=\int_{R=R_{c1}}^{R_{c2}}\int_{\theta=0}^{2\pi}\left[\frac{R}{D_0-W_0(1-R^2)^2}\right]\mathrm{d}R\mathrm{d}\theta$$

$$=\pi\left\{\frac{a\tanh\left[\sqrt{\frac{W_0}{D_0}}\left(R_{c2}^2-1\right)\right]-a\tanh\left[\sqrt{\frac{W_0}{D_0}}\left(R_{c1}^2-1\right)\right]}{\sqrt{W_0D_0}}\right\} \tag{6}$$

The center deflection, W_0, can be replaced by one of the Eq. (1) or Eq. (2), depending on the existence of large deformations and pre-stresses. For the square membranes, no analytical solutions exist so that the integrals must be computed numerically.

4.3. The hydraulic resistance

A pressure drop, related to the flow-rate, is obtained by energy dissipation in the resistance channel between the two pressure sensors. In our design, this is simply implemented by a narrowing of the channel cross-section. The pressure drop over a channel with an effective diameter, d_{eff}, is given by Eq. (7) [11,12]. The used parameters are described in Table 3.

$$\Delta p=f\frac{\rho v_{\mathrm{eff}}^2}{2d_{\mathrm{eff}}}l \tag{7}$$

In our applications, we assumed a rectangular shape of the resistor cross-section. The correction factor for this geometry [12] results in:

$$\Delta p=\frac{1}{8}\left(\frac{\rho v_{\mathrm{eff}}^2}{\mathrm{Re}}\right)\left(\frac{k_{dh}\wp}{S}\right)l. \tag{8}$$

This equation shows the flow dependent and geometry dependent relation of the pressure drop. With the definition of the Reynolds number according to Eq. (9), and substituting this in the flow dependent part, Eq. (10) is obtained.

$$\mathrm{Re}=\frac{\rho v_{\mathrm{eff}}d_{\mathrm{eff}}}{\mu} \tag{9}$$

$$\Delta p=\frac{1}{8}\left(\mu\frac{v_{\mathrm{eff}}}{d_{\mathrm{eff}}}\right)\left(\frac{k_{dh}\wp}{S}\right)l \tag{10}$$

It is shown that the flow-sensor will measure the volume flow and is sensitive to viscosity changes. These aspects will be discussed further on in this article.

Table 3
Used parameters and their units for the fluid computations

Description	Dimensional parameter	Units
Displaced volume	$\forall$	m^3
Volume flow-rate	ϕ	$m^3\ s^{-1}$
Kinematic viscosity	ν	$m^2\ s^{-1}$
Mass density	ρ	$kg\ m^{-3}$
Wetted perimeter	$\wp$	m
Pressure drop	Δp	$N\ m^{-2}$
Thermal expansion coefficient	$\alpha\tau$	K^{-1}
Dynamic viscosity	μ	$Ns\ m^{-2}$
Channel width	a	m
Channel depth	b	m
Hydraulic capacitance	C_{hyd}	$N^{-1}\ m^5$
Effective diameter	d_{eff}	m
Hydraulic diameter	d_{h}	m
Hydraulic power consumption	$\dot{E}$	W
Friction factor	f	–
Resonance frequency	f_{hyd}	Hz
Hydraulic transfer function	G_{hyd}	–
Temperature–viscosity constant	k_{μ}	–
Volume expansion coefficient	k_{ρ}	K^{-1}
Laminar friction constant	k_{dh}	–
Minor loss coefficient	k_{m}	–
Specific heat capacity	k_{T}	$J\ kg^{-1}\ K^{-1}$
Channel length	l	m
Hydraulic inertance	L_{hyd}	$Ns^2\ m^{-5}$
Quality factor	Q_{hyd}	–
Reynolds number	Re	–
Hydraulic resistance	R_{hyd}	$Ns\ m^{-5}$
Cross-section area	S	m^2
Time	t	s
Temperature	T	K
Effective velocity	v_{eff}	$m\ s^{-1}$

The HF etched channels in our sensor were relatively long and wide compared to the depth. In a first approximation we neglected the entrance and exit effects as well as the rounded corners, created during the isotropic etching process. The channel cross-section was assumed to be square. For this situation, the resistance can be described by Eq. (11). The parameters a and b are the side lengths of the cross-section. The friction constant can be obtained empirically and is found in literature [12]. Finally, the volume flow-rate can be extracted from the pressure drop with use of Eq. (12).

$$R_{\mathrm{hyd}}=\frac{\mu}{512}\left(\frac{k_{dh}^2(a+b)^2}{a^3b^3}\right)l \tag{11}$$

$$\phi=\frac{\Delta p}{R_{\mathrm{hyd}}} \tag{12}$$

In this case, the measured pressure signal is linearly related to the flow-rate. The entrance and exit effects however cause so-called minor losses, which introduce a nonlinear behavior as is described by Eq. (13).

$$\Delta p_{\mathrm{minor}}=\frac{1}{2}\rho v_{\mathrm{eff}}^2k_{\mathrm{m}} \tag{13}$$

For the situation of the resistance channel, the minor loss coefficient, k_m, can be as high as 0.5. The relative influence of the minor losses compared to the constant channel resistance is expressed in Eq. (14). This nonlinearity ratio represents the validity of neglecting the minor losses.

$$\frac{\Delta p_{\text{minor}}}{\Delta p_{\text{major}}} = 256\frac{\phi}{\nu}\frac{k_m}{k_{dh}^2}\frac{ab}{(a+b)^2 l} \qquad (14)$$

For flow-rates on the order of a few microliters per second, a kinematic viscosity of about 10^{-6} m^2 s^{-1}, an equal width and depth of the channel and a channel length of a few millimeters, the ratio will be less than 1%. Increasing the channel length can further reduce the non-linear effect of the minor losses. In Fig. 7, the measured and calculated pressure drop are shown as a function of the flow-rate in case water is used. As expected, the nonlinearity is very small and not noticeable. The difference between the measured and computed resistance is substantial (21%). The reason for this might be found in the cross-section geometry and roughness of the resistor channel. We assumed a smooth, rectangular geometry whereas pictures of the channel show a rounded trapezium shape. These rounded corners reduce the net effective cross-section area, which means an increase in resistance. Since the cross-section parameter influences the resistance to the power four as was shown in Eq. (11), this substantial difference between the measurements and computed resistance can easily be obtained: a 21% resistance difference is caused by a net dimension difference of 4.8%

If only major losses are taken into account, the hydraulic energy dissipation per unit time (power) is:

$$\dot{E}_{\text{hyd}} \approx \Delta p_{\text{major}}\phi = R_{\text{hyd}}\phi^2 \qquad (15)$$

This loss of hydraulic energy is converted to thermal energy and thus will rise the fluid temperature. Under the assumption that the heat is only transferred uniformly to the fluid without losses to the channel walls, this temperature rise is given by:

$$\Delta T = \frac{\phi R_{\text{hyd}}}{\rho k_T} \qquad (16)$$

For a sensor design, used in combination with ethanol, resulting in a hydraulic resistance of 1.7×10^{12} Ns/m^5, with a density of 787 kg/m^3, heat capacity of 2.44×10^3 J/kg K and used to measure flows of 1 μl/s, the dissipated energy is 1.70 μW. Since this dissipated energy will heat up the liquid only 8.9×10^{-4} K, the effect is negligible. It shows that the pressure/flow-sensor can be designed to consume besides electrical power, little hydraulic power as well.

5. Modeling of the dynamic sensor behavior

When the sensor is operated in a system with fast fluctuating fluid speeds, it is important to know the dynamics. An example of such application would be to sense the flow-rate produced by a membrane pump. The dynamic behavior of the sensor is important to predict the time dependent signal from the delivered flow and pressure. Due to the dynamic impedance of the sensor, a frequency dependent amplitude change and phase shift of the pressure signal, described by the transfer function, can occur. Transfer functions are based on the assumption of harmonic flows. In practice it is difficult to obtain this situation, but if a linear system is assumed, other, non-harmonic flows can be modeled by using Fourier series. A good indication about the dynamic behavior in the frequency domain can be obtained, which is used to estimate the working range of the sensor. Besides the computed hydraulic resistance of the channel, the sensor consists of

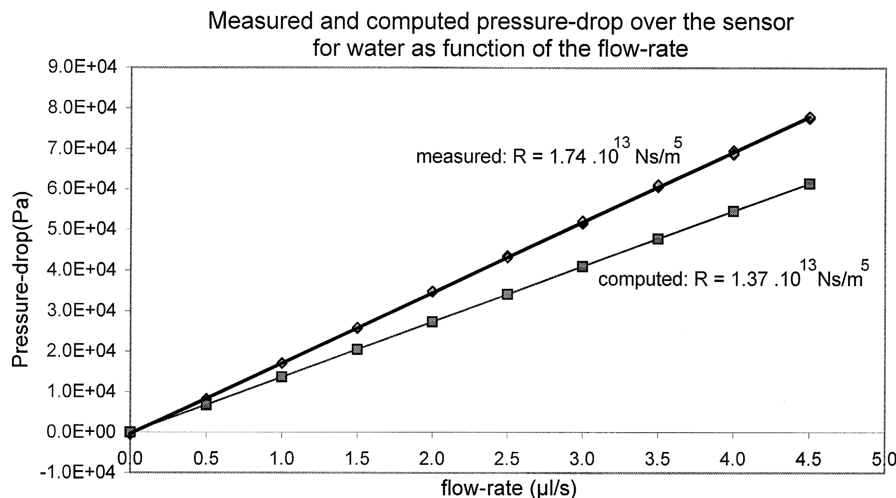

Fig. 7. Measured pressure-drop/flow-rate relation of the sensor. The non-linear entrance and exit effects are negligible.

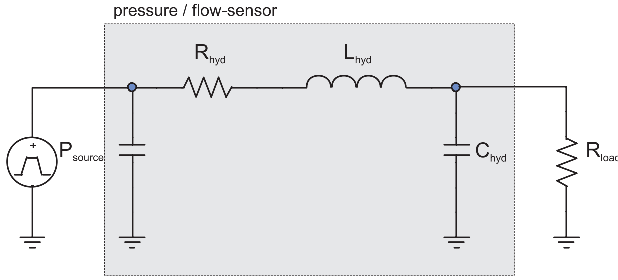

Fig. 8. Electric analogy of the pressure/flow-sensor, simulated with a PSPICE model: the resistance, capacitance and inertance of the sensor. The sensor is fed by a pressure source and loaded by a resistance impedance.

hydraulic capacities and inertance [13] also. In Fig. 8, a schematic of the electronic analogy is drawn.

The pressure sensors form the hydraulic capacities of the sensor. Due to the membrane deflection under a pressure load, liquid can be accumulated. In general, the hydraulic capacity C_{hyd} is described by:

$$\phi = C_{\mathrm{hyd}} \frac{\mathrm{d}p}{\mathrm{d}t}. \tag{17}$$

Since the flow rate is defined as the amount of transported volume per time, the capacitance is defined as the volume change per unit pressure variation:

$$C_{\mathrm{hyd}} = \frac{\mathrm{d}\forall}{\mathrm{d}p}. \tag{18}$$

The volume under a square membrane is given by integrating the dimensionless deflection formula (4).

$$\forall = \int_{-1}^{1}\int_{-1}^{1} \frac{Q}{K_{\mathrm{b}}} (1-X^2)^2 (1-Y^2)^2 \mathrm{d}X\mathrm{d}Y = \frac{256}{225}\frac{Q}{K_{\mathrm{b}}} \tag{19}$$

The capacity for the small deflections of a square membrane will be:

$$C_{\mathrm{hyd}} = \frac{256}{225}\frac{a^6}{Eh^3}\frac{1}{K_{\mathrm{b}}} = 0.28\frac{a^6}{Eh^3}(1-\nu^2). \tag{20}$$

It is assumed that both pressure sensors are identical such that the capacities at both sides of the resistance channel are identical.

Inertance of the sensor is caused by the acceleration of liquid mass in the sensor. Because the fluid velocity under the sensor membranes is assumed to be much smaller than the velocity in the hydraulic resistor, the kinetic energy is regarded to be concentrated in the resistor. Therefore, only the inertance in the resistor channel is taken into account. The hydraulic inertance, L_{hyd}, is defined by equation:

$$\Delta p = L_{\mathrm{hyd}} \frac{\mathrm{d}\phi}{\mathrm{d}t}. \tag{21}$$

According to Newton's second law, the force per area needed to accelerate a plug of liquid with length l and cross-section area S equals:

$$\Delta p = \frac{\rho l}{S}\frac{\mathrm{d}\phi}{\mathrm{d}t} \tag{22}$$

Hence the inertance of the filled channel with rectangular geometry (width × depth = $a \times b$) is defined by:

$$L_{\mathrm{hyd}} = \frac{\rho l}{S} = \frac{\rho l}{ab} \tag{23}$$

The lumped element analogy of the electric circuit indicates that a second order system is to be expected. This electric equivalent circuit is shown in Fig. 8. The complex transfer function of a LRC circuit is expressed in Eq. (24). It shows that only the capacitance of the downstream pressure sensor is of importance.

$$G_{\mathrm{hyd}} = \frac{1}{1 + j\omega R_{\mathrm{hyd}} C_{\mathrm{hyd}} - \omega^2 L_{\mathrm{hyd}} C_{\mathrm{hyd}}} \tag{24}$$

For this second-order system, resonance is to be expected for the LC combination at a frequency f_{hyd} that satisfies Eq. (25) with a quality factor Q_{hyd} expressed by Eq. (26).

$$f_{\mathrm{hyd}} = \frac{1}{2\pi\sqrt{L_{\mathrm{hyd}} C_{\mathrm{hyd}}}} \tag{25}$$

$$Q_{\mathrm{hyd}} = \frac{1}{R_{\mathrm{hyd}}}\sqrt{\frac{L_{\mathrm{hyd}}}{C_{\mathrm{hyd}}}} \tag{26}$$

The prototypes of the capacitive pressure/flow-sensor consist of square silicon membranes of about 25 μm thickness and a length and width of 1500 μm. The hydraulic capacity of these membranes will be around 1.7×10^{-17} m^5/N. For the channels, three different widths are chosen: 200, 340 and 570 μm. The length is 2900 μm and the depth 21 μm. For the 340 μm wide channel, the resistance for ethanol becomes 1.7×10^{12} Ns/m^5 with an inertance of $3/2 \times 10^8$ Ns^2/m^5. With these values, the resonance frequency is 2.2 kHz with quality factor 2.56. When the channel width is varied, the resistance and inertance will be affected. Figs. 9 and 10 show the computed amplitude and phase angle, respectively, of the transfer curves for the three different channel sizes.

From the equations, derived for the dynamic transfer of the sensor, it can be concluded that the current sensor design can be used dynamically with a fluid frequency up to about 1 kHz. If a higher dynamic range is wanted, the resonance frequency must be increased. If we look at Eq. (25), this is possible by reducing the hydraulic capacity or the inertance. The first parameter depends on the pressure sensor design. A reduction of the hydraulic capacity means that a more stiff membrane must be used which has consequences for the electric behavior: smaller gap sizes are needed between the upper and lower electrodes to gain

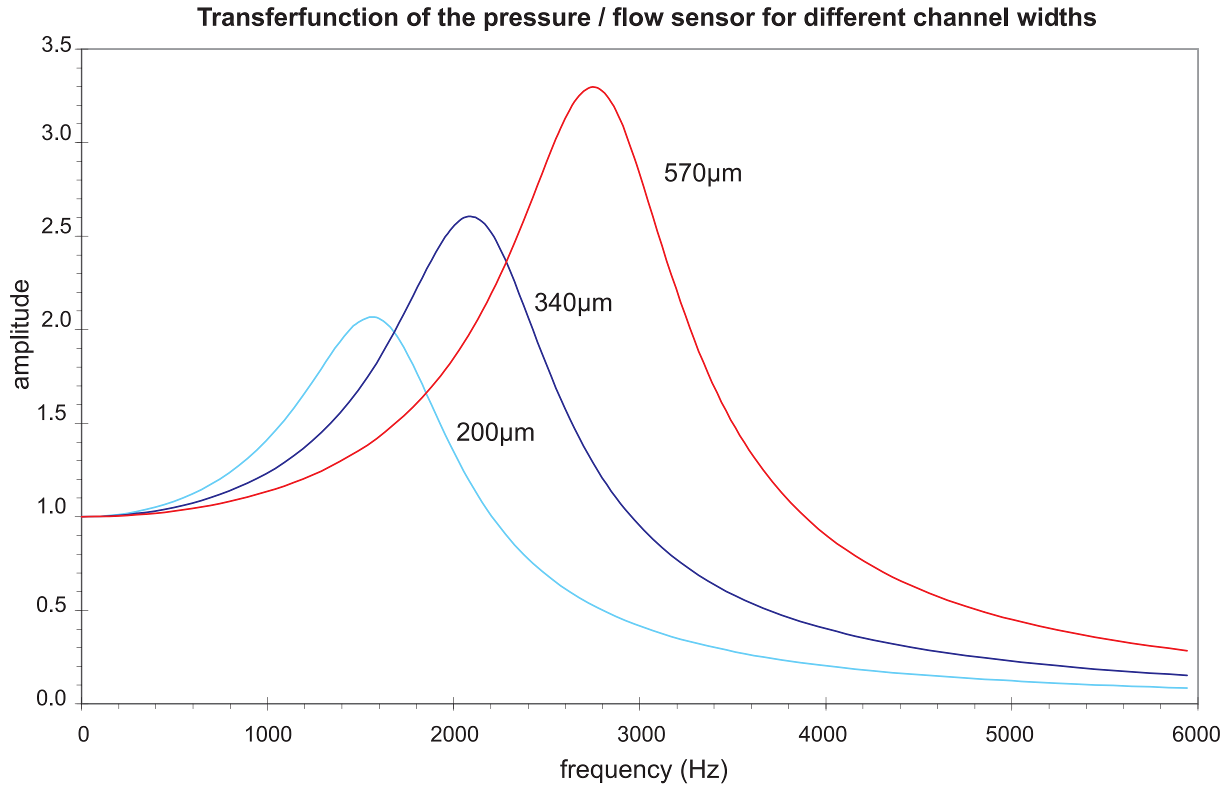

Fig. 9. Computed amplitude of the hydraulic transfer of the fabricated pressure/flow-sensor as function of the driving frequency.

the same pressure sensitivity. When commercial dies are used for the pressure sensors, as for the piezo-resistive variant, the resistance channel can be varied, causing a change of the inertance but hydraulic resistance as well. Variation of the channel dimensions such that the resistance is kept within a pre-defined range, defined by the

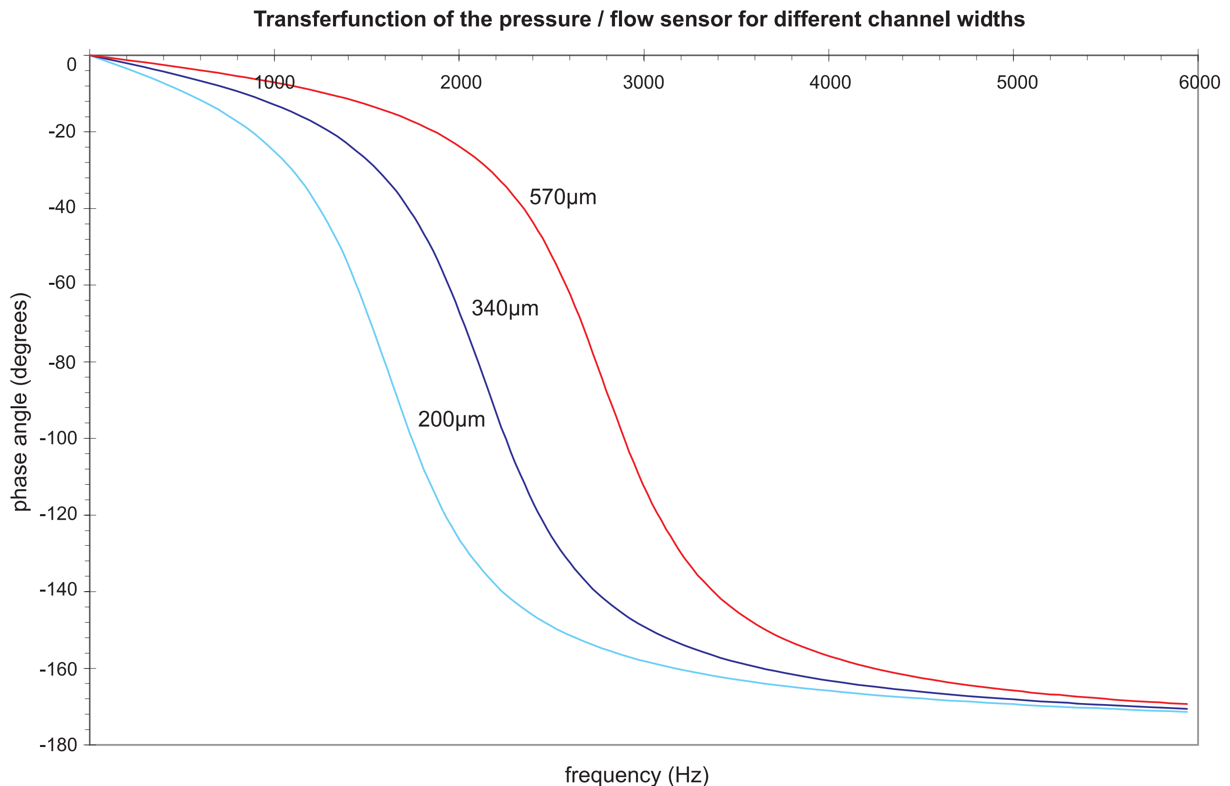

Fig. 10. Computed phase angle of the hydraulic transfer of the fabricated pressure/flow-sensor as function of the driving frequency.

sensitivity of the pressure sensors, and reducing the inertance can be the subject of optimization. A boundary condition in this is the length of the channel, which needs to be long enough to reduce the nonlinear effects of the entrance and exit resistance.

6. Accuracy and stability

Temperature changes can have strong influences on the stability of the sensor. The main influence of temperature variations on the sensor signal is due to a change of density and viscosity as temperature varies. For liquids, the absolute viscosity decreases with increasing temperature. This temperature dependent viscosity change [12] can be approximated for many liquids with the relation:

$$\frac{\mu(T)}{\mu_{293\,\mathrm{K}}} = \exp\left[k_{\mu}\left(\frac{293}{T} - 1\right)\right] \tag{27}$$

Temperature viscosity constants, k_{μ}, vary for different liquids. For ethanol for example this value is 5.72. At around 293 K, the relative change in viscosity will be about 2%/K. This influence of temperature on the viscosity will affect the sensor signal with the same amount because the viscosity is linearly related to the pressure drop as was shown by Eq. (11). This influence has consequences for the stability of the sensor. For high accuracy, the temperature of the liquid must be known or be controlled. For the first prototypes, no high precision was aimed at and thus no temperature regulation or sensing system was implemented. It can be concluded that for an uncompensated sensor, the sensor signal will give an underestimation of the ethanol volume flow rate of about 2%/K increase.

If we want to know the mass flow, the sensor volume flow signal must be multiplied with the mass density of the fluid. This density will vary with temperature according to [12]:

$$\frac{\rho(T)}{\rho_{293\,\mathrm{K}}} = \frac{1}{1 + k_{\rho}(T - 293)} \tag{28}$$

Specific values for the volume expansion coefficient, k_{ρ}, are around 110×10^{-5}/K for ethanol, so that the change in mass density will be about 0.1%/K. If temperature rises, the density will decrease. The temperature induced density variation of ethanol will thus cause an underestimation of the mass flow rate of 0.1%/K temperature increase.

Besides the change in fluid properties, the geometry changes of the sensor also affect the hydraulic resistance. Since the resistance is inversely related to the channel cross-section with the fourth power, small variations in channel size will affect the resistance substantially and thus give deviations in measured pressure drops. The influence of the channel geometry can be expressed by the first derivative of the resistance to the geometry parameter. For simplicity, the situation of a circular channel is taken such that the resistance is inversely related to the fourth power of the diameter. The relative resistance change will thus be defined by:

$$\frac{1}{R_{\mathrm{hyd}}}\frac{\mathrm{d}R_{\mathrm{hyd}}}{\mathrm{d}d_{\mathrm{h}}} = -\frac{4}{d_{\mathrm{h}}} \tag{29}$$

The linear thermal expansion coefficient α_{T} of the used glass (Hoya SD-2) is $3.2 \times 10^{-6}\ \mathrm{K}^{-1}$. This means that the relative resistance change will be:

$$\frac{1}{R_{\mathrm{hyd}}}\frac{\mathrm{d}R_{\mathrm{hyd}}(T)}{\mathrm{d}T} = \frac{1}{R_{\mathrm{hyd}}}\frac{\partial R_{\mathrm{hyd}}}{\partial d_{\mathrm{hyd}}}\frac{\mathrm{d}d_{d_{\mathrm{hyd}}}}{\mathrm{d}T} = -4\alpha_{\mathrm{T}} \tag{30}$$

Substituting α_{T}, gives a resistance change of only 1.28×10^{-3}%. Hence the resistance change due to temperature induced geometry variations is negligible compared to the viscosity and density changes of the fluid. Other mechanisms such as pollution of the sensor, causing coverage of the channel walls can give rise to serious malfunctioning. Also, clogging-up of the channel when particles are involved is disastrous.

7. Conclusions and discussion

A combination of a pressure and flow-sensor, based upon the principle of measuring the pressure drop over a hydraulic resistor, was discussed. The interesting aspect of this pressure/flow-sensor is that the principle is rather simple. It is comparable to measuring currents in an electrical circuit by sensing the voltage drop (= pressure drop) over a fixed resistance.

A few points make the sensor very suitable for micro fluid handling systems: Unlike many thermal mass flow-sensors [3], the electrical contacts of the pressure/flow-sensor are fully galvanic insulated from the fluid. There are no heater and sensor elements in electrical contact with the medium due to which a voltage drop may occur between the fluid and ground. For medicine dosing or some chemical analysis applications, this can be an important requirement. It also facilitates integration with other components, which lack galvanic insulation.

A second feature is the fact that no energy injection in the liquid is used. Only a little energy (μW) is extracted from the fluid stream due to friction. This means that heating up of the fluid is negligible which is an important issue for temperature sensitive materials or chemical reactions. The fact that there is only a little power consumed from the flow to obtain a pressure drop means that no additional electrical energy is needed to generate an actuator signal. These signals, like the heat transfer to the fluid in a thermal flow-sensor, usually consist of much energy.

Using a combination of capacitive pressure sensors further reduces the power consumption, which makes the sensor very suitable in low power applications.

The robustness of the sensor is rather high since there are no fragile bridges in the sensor, like the structures needed in many thermal flow-sensors. Membranes are the weakest structures used. They however are designed to withstand the maximum expected pressures and are no obstacle in the flow path. A final positive feature of the sensor is the reduction of the electronics needed for read-out. The electronics needed to read-out the pressure is also needed to measure the flow. So the same kind of electronics can be used or an additional multiplexer to read-out the second pressure sensor.

Besides these strong points, there are some weak points to consider. The mentioned positive aspect of a passive sensor also has a drawback. If the sensor is used in a system with for example micropumps to deliver flow at a certain pressure, these pumps must compensate the energy loss in the sensor due to friction. A good hydraulic resistance design, combined with sensitive pressure sensors can minimize this drawback.

With the principle of differential pressure flow sensing, the volume flow-rate instead of mass flow-rate is measured. For chemical analysis however, knowledge of mass flow is needed. Therefore, the mass density must be known in order to compute the mass flow. Another parameter that must be known to be able to derive the volume flow out of the pressure difference, is the viscosity. Changing the concentrations of the medium might affect both density as well as viscosity. These effects must be known in order to derive good volume flow values. Temperature changes of the fluid give rise to substantial fluctuations in viscosity. For ethanol at room temperature, this is 2% pressure change per Kelvin. Consequently fluid temperature measurements must be measured and/or controlled to reach a high flow measurement precision. On the longer term, the hydraulic resistance can change due to pollution. Therefore, like many thermal mass flow-sensors, the functionality is hampered when the walls get coated. Particles also form a severe threat because they can clog the resistance channel.

For the micromachined sensor design, presented in this paper, formulas are derived to predict the static as well as dynamic behavior. Because of the presence of hydraulic resistance, inertance and capacitance, the device will act as a damped second order system with a resonance frequency in the range of a few kHz when ethanol is used as a fluid medium. Optimizing the hydraulic pressure sensor capacitance and channel geometry can increase this range.

These sensor aspects lead to the conclusion that the pressure/flow-sensor is simple and low power consuming dynamic fluid sensing device, capable of measuring both parameters, describing the hydraulic domain: pressure and flow-rate. If no temperature compensation is applied, the application area will be low precision flow rate measurements. When temperature is known or controlled, high precision is possible.

References

[1] A. van den Berg, T.S.J. Lammerink, Micro Total Analysis Systems: Microfluidic aspects, integration concept and applications, in: A. Manz, H. Becker (Eds.), Microsystem Technology in Chemistry and Life Science, Topics in Current Chemistry, Vol. 194, Springer, Berlin, 1998, pp. 21–49.

[2] M. Elwenspoek, T.S.J. Lammerink, R. Miyake, J.H.J. Fluitman, Towards integrated microliquid handling systems, J. Micromech. Microeng. 4 (1994) 227–245.

[3] T.S.J. Lammerink, N.R. Tas, M.C. Elwenspoek, J.H.J. Fluitman, Micro-liquid flow sensor, Sensors and Actuators A, 1993 pp. 45–50.

[4] S. Shoji, M. Esashi, Microflow devices and systems, J. Micromech. Microeng. 4 (1994) 157–171.

[5] J. Franz, H. Baumann, H.P. Trah, A silicon microvalve with integrated flow sensor, Int. Conf. on Solid-State Sensors and Actuators, 1995 pp. 313–316.

[6] M. Esashi, S. Eoh, T. Matsuo, S. Choi, The fabrication of integrated mass flow controllers, Int. Conf. on Solid-State Sensors and Actuators, 1987, pp. 830–833.

[7] P. Gravesen, J. Branebjerg, O. Søndergård Jensen, Microfluidics—a review, J. Micromech. Microeng. 3 (1993) 168–182.

[8] M.A. Boillat, A.J. van der Wiel, A.C. Hoogerwerf, N.F. de Rooij, A Differential Pressure Liquid Flow Sensor for Flow Regulation and Dosing Systems, Proc. IEEE MEMS'95, The Netherlands, 1995 pp. 350–352.

[9] S.P. Timoshenko, S. Woinowsky-Krieger, Theory of plates and Shells, 2nd edn., McGraw-Hill, New York, 1970.

[10] J.Y. Pan, P. Lin, F. Maseeh, S.D. Senturia, Verification of FEM analysis of load-deflection methods for measuring mechanical properties of thin films, Tech. Digest IEEE Solid-State Sensors Workshop, 1990, pp. 70–73.

[11] R.W. Fox, A.T. McDonald, Introduction to Fluid Mechanics, 3rd edn., Wiley, New York, 1985.

[12] F.W. White, Fluid Mechanics, 3rd edn., McGraw-Hill, New York, 1994.

[13] T.S.J. Lammerink, N.R. Tas, J.W. Berenschot, M.C. Elwenspoek, J.H.J. Fluitman, Micromachined hydraulic astable multivibrator, Proc. IEEE MEMS'95, The Netherlands, 1995, pp. 13–18.

Rijk Edwin Oosterbroek, call name 'Edwin', was born in Borne, The Netherlands, on January 28, 1970. He received his MSc degree in Mechanical Engineering from the University of Twente, Enschede, The Netherlands, in 1994. During his graduation time, he joined the Structures and Materials department of the Dutch National Aerospace Laboratory, NLR. In this period, he worked on optimization of dynamic finite element models with use of measured frequency response data. During his civil service, Edwin explored the world of microsystem technology at the MESA Research Institute, University of Twente, Electrical Engineering department, during which he was involved in the micro-pump project. In 1995 he started his PhD project at the same Transducer Technology group, where he studies devices and simulation tools for micro fluid control.

Theo Lammerink was born in Tubbergen, the Netherlands, October 1956. He received his Masters degree in Electrical Engineering and his PhD from the University of Twente, in 1982 and 1989, respectively. His PhD research was focused on the optical excitation and read-out of micromechanical resonator sensors. He is member of the Transducer Technology group of the MESA research institute. His research interests are on micro liquid handling systems and integrated electromechanical micro systems.

J.W. Berenschot, call name 'Erwin', was born on December 13, 1967, in Winterswijk, The Netherlands. He received the BSc degree in applied physics from the Technische Hogeschool Enschede in 1990. Since 1992, he is employed at the Transducer Technology group of the MESA Research Institute. His main research area is fabrication technology with emphasis on developing and characterizing of etching and deposition techniques for the fabrication of micro systems.

Gijs J.M. Krijnen was born 1961, in Laren, the Netherlands. He received his MSc degree in Electrical Engineering from the University of Twente following a study on magnetic recording carried out at the Philips Research Laboratories, Eindhoven, The Netherlands. From 1987 to 1992 he carried out his PhD research in the Lightwave Device Group of the MESA Research Institute at the University of Twente. He investigated nonlinear integrated optics devices. In 1992 he became a fellow of the Royal Netherlands Academy of Arts and Sciences and studied second and third order nonlinear integrated optics devices. 1993 he was the recipient of the Veder price of the Dutch Electronics and Radio Engineering Society (NERG). From 1993 to 1994 he was a visiting postdoc at the Center for Research and Education in Optics and Lasers in Orlando, FL. He worked as a postdoc on linear integrated optic devices at the University of Twente and the Delft University of Technology from 1995–1997. In 1998, he started in the Transducer Technology group of the MESA research institute. His current interests include (modeling of) MEMS, MOEMS, micro-fluidics, micro-sensor and micro-actuator devices.

Miko Elwenspoek (born December 9, 1948 in Eutin, Germany) studied physics at the Free University of Berlin (West). His master thesis dealt with Raleigh scattering from liquid glycerol using light coming from a Mössbauer source. From 1977–1979, he worked with Prof. Helfrich on lipid double layers. In 1979 he started his PhD work with Prof. Quitmann on the subject: relaxation measurements on liquid metals and alloys, in particular alkali metal alloys. In 1983, his work resulted in a PhD degree at the Freie Universität Berlin. In the same year, he moved to Nijmegen, The Netherlands, to study crystal growth of organic crystals in the group of Prof. Bennema of the University of Nijmegen. In 1987 Miko went to the University of Twente, to take charge of the micromechanics group of the Sensors and Actuators lab, now called the MESA Research Institute. Since then his research is focused on microelectromechanical systems such as design and modeling of micropumps, resonant sensors and since the beginning of the 1990s more and more attention is given to electrostatic microactuators for microrobots. Fabrication techniques such as the physical chemistry of wet chemical anisotropic etching, reactive ion etching, wafer bonding, chemical-mechanical polishing and the materials science of various thin films receive his special attention. Since 1996 Miko is employed as full professor at the Transducer Technology group at the Faculty of Electrical Engineering of the University of Twente.

Albert van den Berg, born September 20, 1957 in Zaandam, The Netherlands, graduated from the University of Twente in 1983. He started a PhD research at the same university from which he received in 1988 his degree in Technical Sciences on a thesis called 'Ion Sensors Based on ISFETs with Synthetic Ionophores'. After this he became project leader at the Swiss Center of Micromechanics (CSEM) where he was responsible for several sensor projects. From 1991–1993 he joined the University of Neuchâtel as a research scientist in silicon-based electrochemical sensors and microsystems for chemical analysis. After this period he came back at the University of Twente where he became research coordinator for the Micro Total Analysis Systems orientation of the Mesa Research Institute. At this position, he is currently appointed as full professor of the chair Miniaturized (Bio) Chemical Analysis Systems (since 1998). Albert van den Berg is, among others, a member of the NanoTech, and μ-TAS scientific committees.